Two-Dimensional Layered Chalcogenides: From Rational Synthesis to Property Control via Orbital Occupation and Electron Filling

Published as part of the Accounts of Chemical Research special issue "2D Nanomaterials beyond Graphene".

Hongtao Yuan,[†,‡] Haotian Wang,[§] and Yi Cui*,[†,‡,∥]

[†]Geballe Laboratory for Advanced Materials, Stanford University, Stanford, California 94305, United States

[‡]Stanford Institute for Materials and Energy Sciences, SLAC National Accelerator Laboratory, Menlo Park, California 94025, United States

[§]Department of Applied Physics, Stanford University, Stanford, California 94305, United States

[∥]Department of Materials Science and Engineering, Stanford University, Stanford, California 94305, United States

ABSTRACT: Electron occupation of orbitals in two-dimensional (2D) layered materials controls the magnitude and anisotropy of the interatomic electron transfer and exerts a key influence on the chemical bonding modes of 2D layered lattices. Therefore, their orbital occupations are believed to be responsible for massive variations of the physical and chemical properties from electrocatalysis and energy storage, to charge density waves, superconductivity, spin−orbit coupling, and valleytronics. Especially in nanoscale structures such as nanoribbons, nanoplates, and nanoflakes, 2D layered materials provide opportunities to exploit new quantum phenomena.

In this Account, we report our recent progress in the rational design and chemical, electrochemical, and electrical modulations of the physical and chemical properties of layered nanomaterials via modification of the electron occupation in their electronic structures. Here, we start with the growth and fabrication of a group of layered chalcogenides with varied orbital occupation (from 4d/5d electron configuration to 5p/6p electron configuration). The growth techniques include bottom-up methods, such as vapor−liquid−solid growth and vapor−solid growth, and top-down methods, such as mechanical exfoliation with tape and AFM tip scanning.

Next, we demonstrate the experimental strategies for the tuning of the chemical potential (orbital occupation tuned with electron filling) and the resulting modulation of the electronic states of layered materials, such as electric-double-layer gating, electrochemical intercalation, and chemical intercalation with molecule and zerovalence metal species. Since the properties of layered chalcogenides are normally dominated by the specific band structure around which the chemical potential is sitting, their desired electronic states and properties can be modulated in a large range, showing unique phenomena including quantum electronic transport and extraordinary optical transmittance.

As the most important part of this Account, we further demonstrate some representative examples for the tuning of catalytic, optical, electronic, and spintronic properties of 2D layered chalcogenides, where one can see not only edge-state induced enhancement of catalysis, quantum Aharonov−Bohm interference of the topological surface states, intercalation modulated extraordinary transmittance, and surface plasmonics but also external gating induced superconductivity and spin-coupled valley photocurrent. Since our findings reflect the critical influences of the electron filling of orbital occupation to the properties in 2D layered chalcogenides, we thus last highlight the importance and the prospective of orbital occupation in 2D layered materials for further exploring potential functionalized applications.
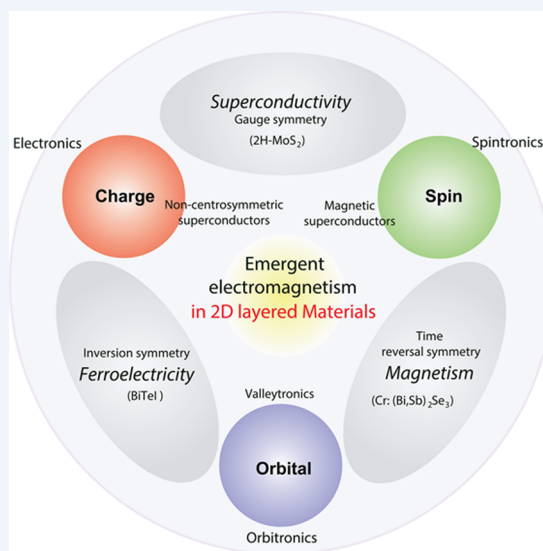
1. INTRODUCTION

Two-dimensional (2D) layered materials have recently attracted much interest due to their unique physical and chemical properties[1−3] as well as potential applications in electronics, optoelectronics, energy storage, and catalysis.[2−4] A wealth of unusual physical phenomena occurs when charges are confined into the 2D lattice. Determined by the Fermi surface and the specific band structure near the Fermi level, their electronic properties can be effectively modified by controlling the electron filling into the
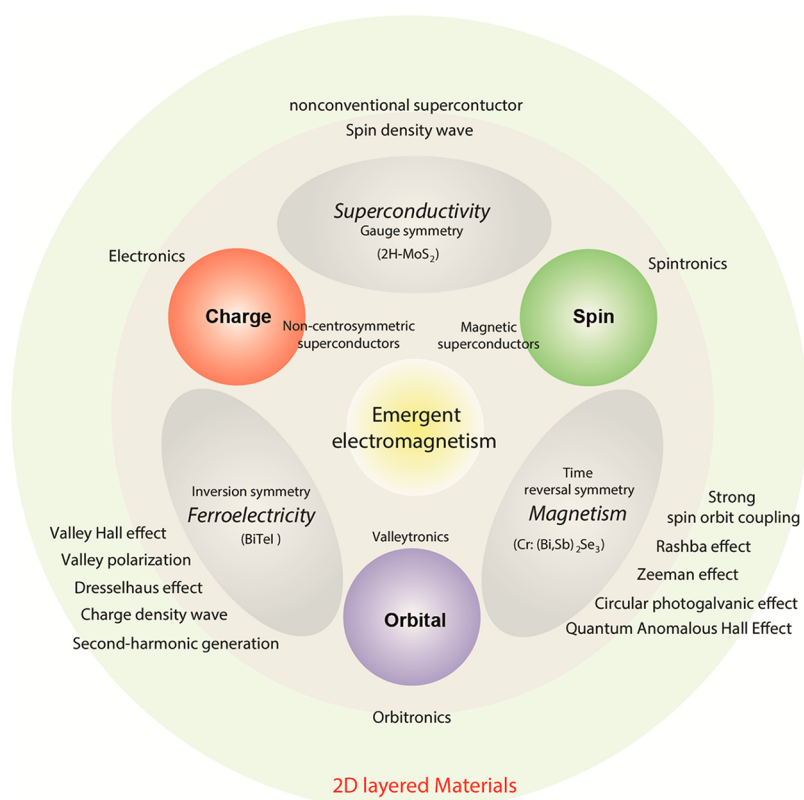
Figure 1. Schematic diagram demonstrating the symmetries and degrees of freedom of electrons confined in 2D layered materials and resulting emergent phenomena that can be engineered in the layered materials.[6]

orbitals. Figure 1 shows the schematic diagram for the symmetries and degrees of freedom of electrons that can be engineered in 2D layered materials for many emergent phenomena.[5] For example, spatial variations of the d-orbital occupation are known to generate a multitude of electronic phases with radically different macroscopic properties,[5,6] which can bring us unique d-orbital electron filling and anisotropic-shaped d-electron clouds. These have been intensively investigated not only to fundamentally understand the intriguing physics and chemistry in 2D layered materials[7,8] but also to examine their potential applications in novel electrochemical, electronic, and spintronic devices.[9−12] The electron count, used to describe the electron configuration and electron filling in the orbitals in coordination complexes (Figure 2), can serve as an effective indicator to understand the geometry and reactivity of layered materials and also provide us with guidance for property control. The emerging ionic, electronic, spintronic, and photonic phenomena in the confined electronic systems,[3,13,14] such as the topological surface state in topological insulators[15,16] and valley polarization selection in monolayer MoS_2, can be controllably tuned by modifying their electron filling with doping, quantum size effect, field effect, or intercalation of molecules, atoms, and ions into van der Waals layers.

Taking layered transition metal dichalcogenides (TMDs) as examples, Figure 2 shows the evolution of the electronic structures of representative compounds with varying the electron configuration and the coordination environment of metal elements.[2] Considering layered dichalcogenides with trigonal prismatic coordination of the transition-metal (D_{3h}, shown in Figure 2a), the d orbital components d_{z^2}, $d_{x^2−y^2,xy}$, and $d_{xz,yz}$ are split into three independent subbands, with a sizable band gap between d_{z^2} and $d_{x^2−y^2,xy}$ groups.[2] The diverse electronic structures of TMDs arise from the evolving electron filling of the nonbonding d bands

(Figure 2b). For example, TMDs exhibit metallic conductivity when the d_{z^2} orbitals are partially filled in 2H-$TaSe_2$ ($5d^36s^2$ for Ta), while they are semiconductors when the d_{z^2} orbitals are fully occupied in 2H-WSe_2 ($5d^46s^2$ for W). If we further add electrons to fully fill the 5d orbitals by changing the metal to bismuth ($5d^{10}6s^26p^3$ in Bi_2Se_3), since the spin−orbit coupling strength in Bi_2Se_3 is strong enough, the layered compound thus starts to have a "band inversion" and forms a topological surface state in the folded band gap (0.3 eV), as shown in Figure 2c.[16] On one hand, with varying orbital occupation, this gradual evolution of electronic properties from metal, to semiconductor, and to band-folded topological insulators gives us the diversity of physical and chemical properties of 2D layered materials. On the other hand, their materials properties can be continuously tuned by modifying their electron filling with doping, field effect, and intercalation. Reviewed here is our recent progress on the rational control of the chemistry and physical properties of 2D layered nanostructures via orbital occupation with electron filling.

2. RATIONAL SYNTHESIS

The reliable growth of high quality 2D materials with desired dimensionality is an essential first step for realizing materials with desired orbital occupations and further functionalizing them for device applications.

Vapor−liquid−solid (VLS) growth is one of the most important synthetic methods for 2D layered nanoribbons and nanowires.[17] The target materials are transported by carrier gas downstream where substrates are located (Figure 3). Before the growth, metal nanoparticles, Au nanoparticles in most cases, are first uniformly predeposited onto the substrates to act as the catalysts for nanoribbon growth.[17,18] There are many successful examples of 2D layered nanoribbon and nanowire syntheses
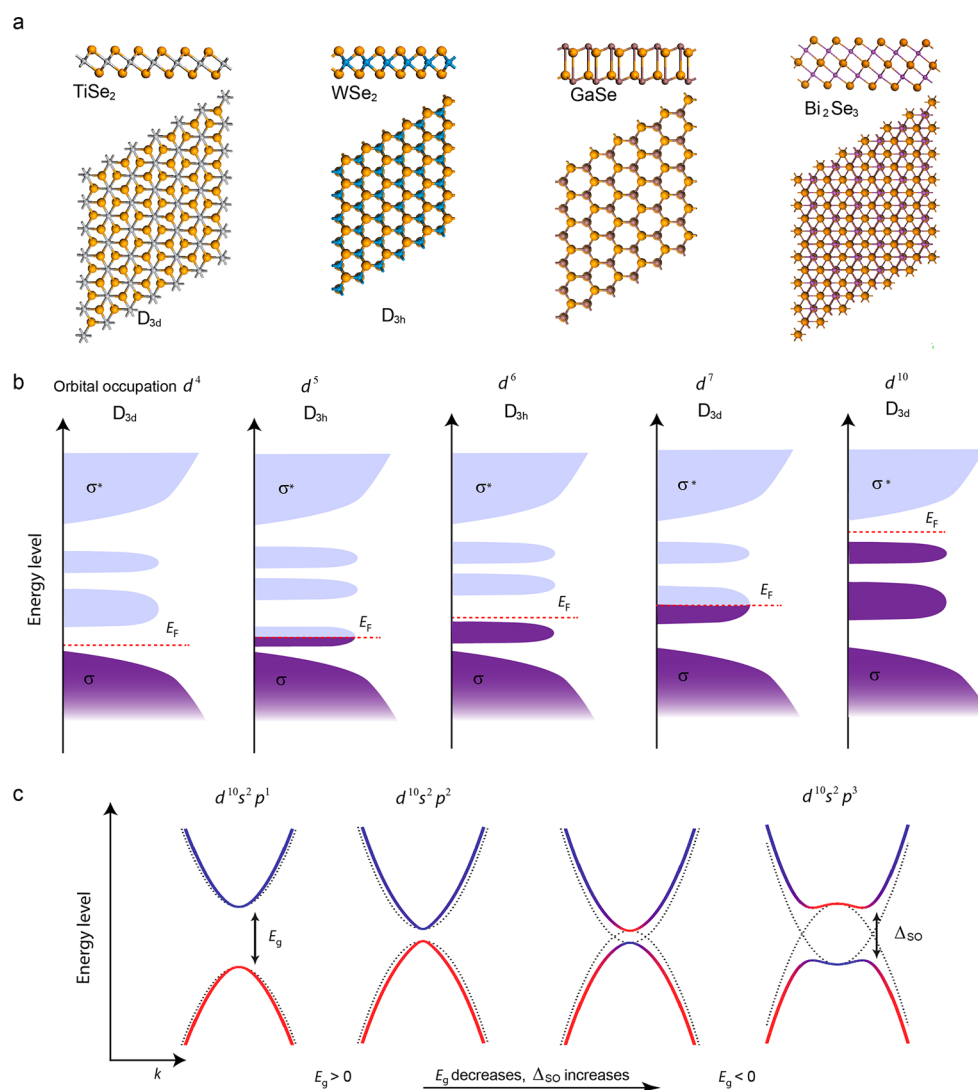
Figure 2. (a) Crystal structures of representative layered chalcogenides. (b) Schematic illustration for progressive electron filling of d orbitals in transition metal chalcogenides.[2] (c) Band structure evolution of layered chalcogenides with group III to group V elements, with the band gap evolution from a positive value (a semiconductor) to a negative one (a topological insulator). Panel c reproduced with permission from ref 16. Copyright 2012 American Physical Society.

with this VLS method, including Bi_2Se_3, Bi_2Te_3, and Sb_2Te_3 nanoribbons, In_2Se_3 and Ga_2Se_3 nanowires, and related alloys.[19−24] Figure 3a shows the Bi_2Se_3 nanoribbon growth using Au nanoparticles as the catalyst.[19] A gold nanoparticle present at the end of the ribbon suggests the VLS growth mechanism. The ribbons are single-crystalline rhombohedral phase with atomically smooth edges and flat surface (Figure 3b and 3c). We can achieve VLS growth for In_2Se_3 nanowires along both in-plane and out-of plane directions, confirmed by transmission electron microscopy (TEM). Importantly, the final dimensionality and morphologies of 2D layered nanorib-bons and nanowires can be flexibly controlled by changing the growth temperature and time or the flow rate of carrier gas in VLS synthesis in a desired way (Figure 3d).[22,23] For example, Bi_2Se_3 nanowires, which exhibit rough surfaces, are formed by stacking nanoplates along the axial direction of the wires, and nanoribbons are grown along $[11\bar{2}0]$ direction with a rectangular cross-section and have diverse morphologies, including quasi-one-dimensional, sheet-like, zigzag, and sawtooth shapes.[22]

Different from VLS growth, vapor−solid (VS) syntheses are free of catalyst (Figure 4a). The high anisotropy of 2D

materials plays a critical role in the morphology of nanoplates (Figure 4b).[25] For example, the bonds of 2D atomic layers at the top and bottom surfaces are fully saturated without any dangling bond, which retards the growth rate along the c axis. However, the edge of the layers have dangling bonds where the involved gas phase vapors are preferentially attached, resulting in a signi-ficantly faster growth rate along the in-plane directions. Few-layer ultrathin nanoplates of Bi_2Se_3 and Bi_2Te_3 with thickness down to ∼3 nm were successfully achieved by this VS mechanism on the Si/SiO_2 substrate (Figure 4c).[25,26] The lateral dimensions of the nanoplates extend from several micrometers up to ∼20 μm. Importantly, the ternary alloyed phase $(Bi_xSb_{1−x})_2Te_3$ nanoplates can also be obtained using VS growth using a mixture of Bi_2Te_3 and Sb_2Te_3 powders as precursors.[26] TEM images suggest the single crystallinity of the nanoplates and energy-dispersive X-ray spectroscopy elemental mapping in Figure 4 indicates the uniform distribution of bismuth and antimony across the entire nanoplate without detectable phase separation.

Solid state reaction provides another possibility for binary nanostructure growth using reactions of layered compounds with other desired elements (Figure 5).[27,28] By heating the In_2Se_3
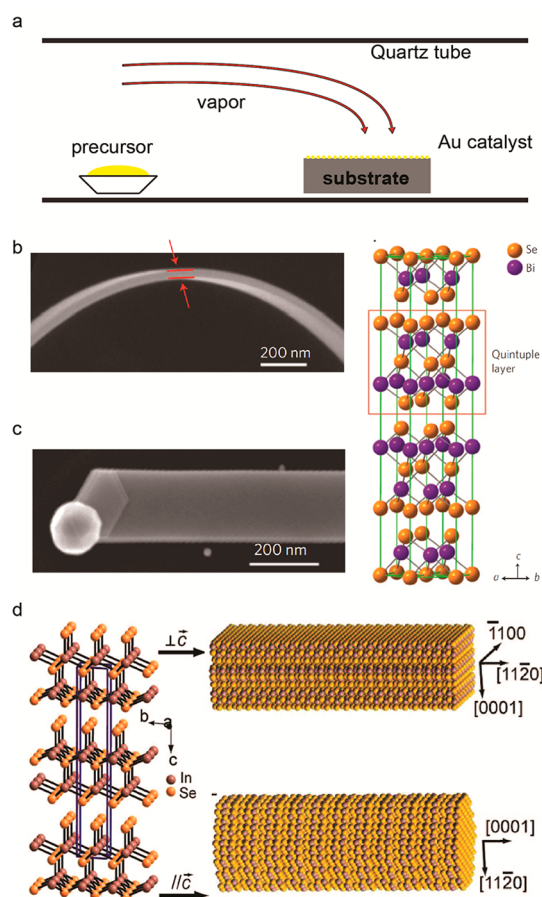
Figure 3. (a) Schematic mechanism of VLS synthesis of layer nanoribbons and nanowires. (b, c) SEM images of Bi_2Se_3 nanoribbons with Au nanoparticles as the catalyst. Reproduced from ref 19. Copyright 2010 Nature Publishing Group. (d) Schematic of In_2Se_3 nanowire growth along different directions. Reproduced from ref 20. Copyright 2008 American Chemical Society.

Figure 4. (a) Schematic mechanism of VS synthesis and anisotropic growth of nanoplates. Reproduced from ref 25. Copyright 2010 American Chemical Society. (b) AFM images of Bi_2Se_3 and Bi_2Te_3 nanoplates. Reproduced from ref 25. Copyright 2010 American Chemical Society. (c) Optical microscopy, TEM, and EDX characterizations of ternary $(Bi_xSb_{1-x})_2Te_3$ nanoplates. Reproduced from ref 26. Copyright 2011 Nature Publishing Group.

Figure 5. (a, b) Schematic and optical images for the mechanism of chemical reaction synthesis. (c, d) Schematic structure transformation from In_2Se_3 nanowires to $CuIn_2Se_3$ nanowires. Reproduced from ref 27. Copyright 2009 American Chemical Society.

nanowires for solid-state reaction with copper, we can transform the In_2Se_3 nanowires into high-quality single-crystalline $CuInSe_2$ nanowires. The chemical transformation from In_2Se_3 to $CuInSe_2$ nanowires presents the entire process of the solid state reactions by in situ TEM characterizations.[27,28] Interestingly, the transformation temperature exhibits a surprising anisotropy, with In_2Se_3 nanowires grown along their $[0001]$ direction transforming at a low temperature of 225 °C, while nanowires in a $[11\bar{2}0]$ orientation require a much higher temperature of 585 °C, due to the high anisotropy of the layered materials. These results offer a route to the synthesis of $CuInSe_2$ nanowires at a relatively low temperature as well as insight into the details of a transformation commonly used in the fabrication of thin-film solar cells.

Decades ago, mechanical and chemical exfoliation were tried to achieve layered chalcogenides with few and single layers,[29,30] providing a simple but effective method to fabricate layered materials at their monolayer limit. Even now, "Scotch tape" mechanical cleaving is still the most common approach for obtaining single- and few-layer-thick 2D materials. In addition, we reported a controlled mechanical exfoliation of Bi_2Se_3 nanoribbons by an atomic force microscope (AFM) tip down to single quintuple-layers of Bi_2Se_3 (Figure 6).[31] When the horizontal force applied by the AFM tip is large enough, the upper portion of the ribbon will be scratched away. Therefore, we can remove most of the upper layers and have intact ultrathin
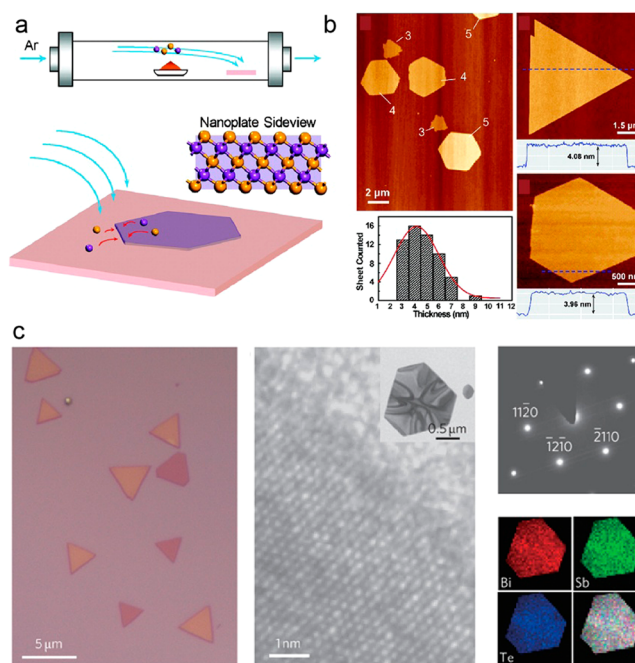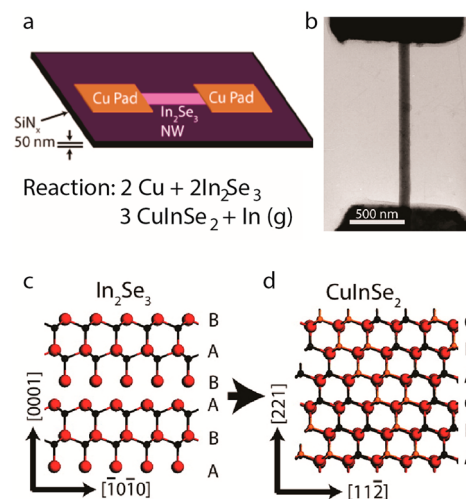
Bi_2Se_3 at the bottom while maintaining the original lateral length of about several micrometers.[31]

3. PHYSICAL AND CHEMICAL METHODS FOR ORBITAL OCCUPATION CONTROL

Since material properties are always associated with their electronic structures, especially the position of Fermi level and the size and shape of Fermi surfaces, continuous electron filling into their orbitals can serve as the most effective way to modulate the electronics states and therefore the physical and chemical
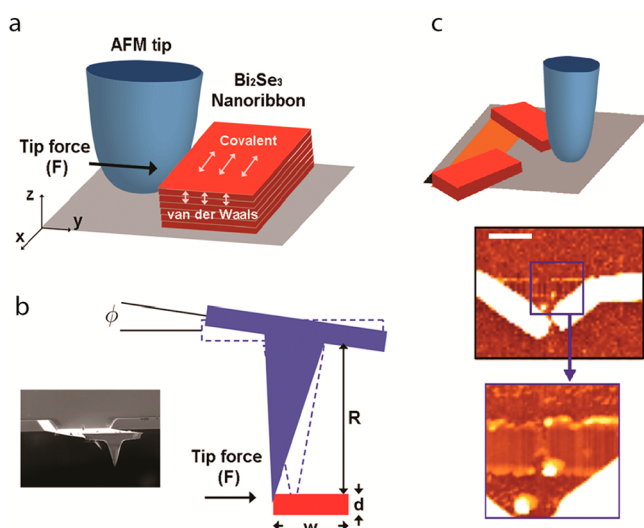
Figure 6. (a) Schematic of AFM exfoliation of layered Bi_2Se_3 nanoribbon. (b) The horizontal tip force is from torsional displacement of the tip. (c) AFM images after breaking by tip exfoliation. Reproduced from ref 31. Copyright 2010 American Chemical Society.

properties of layered materials. With this general guidance, we have successfully used the following techniques to modulate material properties in 2D layered materials.

3.1. Electric-Double-Layer Gating

Electric-field control of charge carrier density has attracted much attention because it is a simple method for modulating the physical properties of materials and for exploring new

functionalities with a transistor configuration. As a functionalized interface, the electric double layer (EDL) interface, working as a nanogap capacitor with a huge capacitance (middle panel of Figure 7a), can accumulate a large amount of charge with low operation voltages, resulting in remarkable advances in high performance EDL transistors[32,33] and electrostatic modulation of electronic states of solids.[34] Therefore, using EDL transistors to electrostatically tune physical properties of 2D chalcogenides is a rather new territory and can bring us to new physical transformations (insulator−metal−superconductor transition, modulation of spin−orbit coupling) and device functionalities (generation of valley current and valleytronics devices). For example, we can easily realize ambipolar operation in WSe_2 and MoS_2 with such EDL gated transistors.[12] Also, by tuning the gate voltage within EDLTs on flakes of layered MoS_2, we observe an electric field induced quantum insulator−superconductor transition. Further investigation clearly indicated a 2D insulator-to-superconductor transition around the pair quantum resistance $h/(2e)^2$ and a dimensional crossover (2D-anostropic 3D) of the gate induced superconductivity in MoS_2.

3.2. Electrochemical Intercalation

As another powerful tool based on electrochemical cells for batteries and supercapacitors, electrochemical intercalation can be used for tuning both the chemical potential and the electronic structure of 2D materials with electron filling. In electrochemical intercalation (right panel of Figure 7a), either cations (such as Li^+, Cu^+, or Ag^+) or anions can be electrochemically intercalated into the van der Waals gap or the crystal lattice or reacted with the crystal in a simple electrochemical reaction ($Li + MoS_2 + e \leftrightarrow Mo + LiS_2$). Intercalation is the change of redox state of host lattice ions, and often the carrier density can be modulated
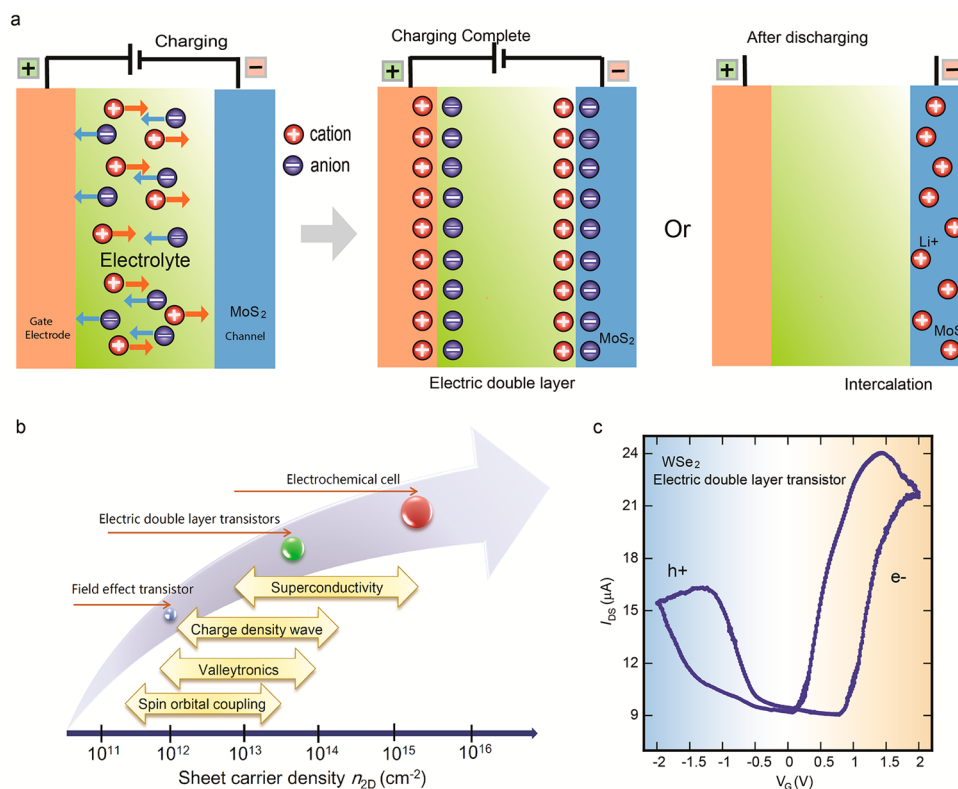

Figure 7. (a) Schematic diagram for electric-double-layer gating (middle panel) and electrochemical intercalation (right panel). (b) Physical phenomena in layered materials as a function of the 2D carrier density. (c) Ambipolar operation of a WSe_2 EDL transistor. Reproduced from ref 54. Copyright 2014 Nature Publishing Group.

significantly compared with electrostatic gating (middle panel of Figure 7a) and therefore drive the electronic state into metallic phase and even superconducting phase.[35] Also, when the concentration of intercalation ions is high enough, it is also possible to induce a structural or phase transformation, which change the electronic band structure completely. Lithium atoms can fill in the layer-like structural vacancies of In_2Se_3 nanowires and generate new types of vacancies and lithium atom ordering superlattices.[36]

3.3. Zerovalent Intercalation

The amount of intercalant that can be inserted into a host material is limited by the charge and size of the guest species and the ability of the host to maintain charge balance and structural stability. The ionic nature of many guest species requires either a change of the host lattice oxidation states or the presence of atomic vacancies to maintain charge neutrality.[37] Though intercalation of alkali metals such as lithium can be high because of their small size, most intercalation concentrations are limited by the ionic nature of the intercalant. A zerovalent intercalant does not require a change in the oxidation state of the host lattice, thus allowing a high intercalation concentration.

We successfully developed a chemical, solution-based method whereby a reaction to generate a zerovalent copper species is performed in the presence of a layered material because zerovalent intercalant does not disrupt the host crystal (Figure 8). High densities, up to 60 atomic percent, of zerovalent copper metal can be intercalated into Bi_2Se_3 nanoribbons, controlled by either the concentration or the reaction time. On one hand, this is general, whereby many other zerovalent metals (such as Cu, Ag, Co, In, Pt, Pd, or Sn) can be intercalated into layered Bi_2Se_3 chalcogenide nanoribbons.[38] On the other hand, such superstoichiometric, zerovalent intercalation can be extended to different 2D host materials, including MoO_3, Sb_2Te_3, In_2Se_3, and GaSe.[39] Besides the above-mentioned intercalation of the ions, zerovalence metals, we can also intercalate large molecules into the layered materials to modify their electron filling and orbital occupation and resulting properties.[40]

4. MODULATION OF CHEMICAL AND PHYSICAL PROPERTY OF 2D MATERIALS VIA ELECTRON FILLING

4.1. Catalytic Properties

In these layered materials hosting d orbitals, the spatial variations of the d-orbital occupation are known to generate a multitude of electronic phases with radically different macroscopic properties[1] and can serve as an effective way to understand the reactivity of layered materials. The Norskov group theoretically revealed that the edge sites of MoS_2 are active in catalyzing the hydrogen evolution reaction (HER) compared with their terrace counterparts[8,41] since the edge sites of 2D layers have unsaturated coordination and dangling bonds, which are believed to serve as active sites to bond H (Figure 9a).[41] We rationally designed an ideal structure of edge-terminated MoS_2 nanofilms with high HER activity (Figure 9b).[42,43] This thermodynamically unfavored structure was successfully achieved by a rapid sulfurizaiton process. Accordingly, layers perpendicular to the substrate are preferentially grown and finally result in the layer vertically standing structure (Figure 9c).[42]

The HER performance of the edge-terminated MoS_2 is shown in Figure 9d with a very large Tafel slope of 120 mV/decade, which indicates the sluggish discharge step of HER.[43] The cathodic current reaches 2 mA/cm² at over 350 mV overpotential. Improvements have been achieved when the edge-terminated $MoS_2/MoSe_2$ nanofilms were translated onto rough
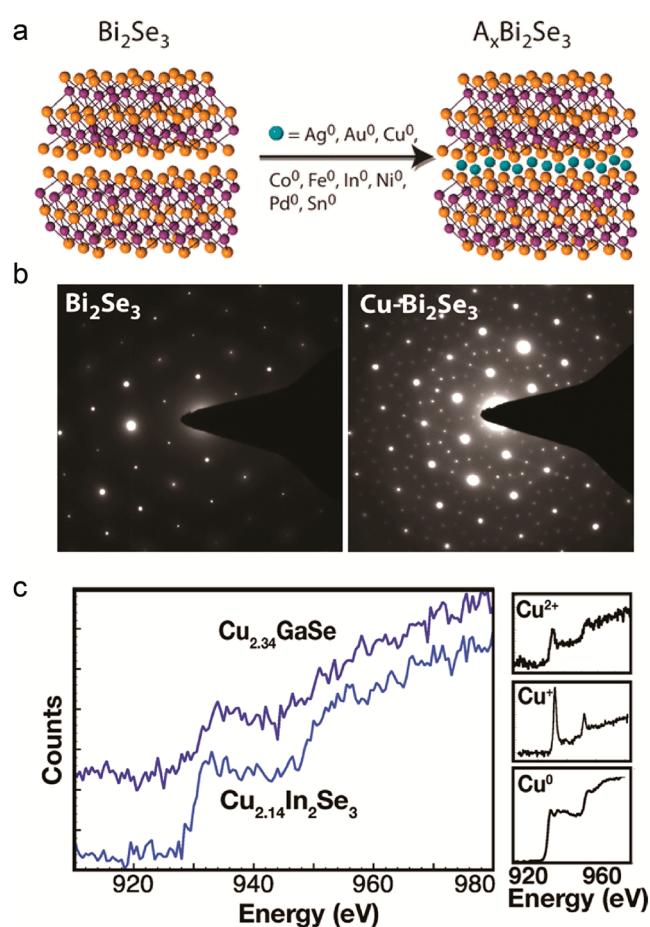

Figure 8. (a, b) Schematic and TEM images for Bi_2Se_3 nanoplates before and after Cu^0 intercalation. Reproduced from ref 37. Copyright 2012 American Chemical Society. (c) EELS fine structure plots, confirming the zerovalent nature of the intercalated copper. Reproduced from ref 39. Copyright 2014 American Chemical Society.

and curved substrates.[43] The Tafel slope was significantly improved from 120 to 60 mV/decade, with HER activity of 10 mA/cm² at only 250 mV overpotential. To further enhance the HER activity, we use Li electrochemical intercalation since both the charge transfer and the layer spacing expansion can change the electronic structure of 2D materials, thus effectively tuning their catalytic activates for optimized electrocatalysis. With the intercalation potential going down, the Mo oxidation states get lower and lower (Figure 9e).[44–47] A transition of semiconducting 2H to metallic 1T phases was observed, resulting in enhanced HER catalytic activities. In addition to HER, the efficacy of the electrochemical tuning method was also successfully demonstrated in 2D material oxygen evolution reaction (OER).[48,49]

4.2. Topological Insulators

The unique orbital occupation, strong spin–orbit coupling and narrow band gap in the electronic structure of Bi_2Se_3, with the electron occupation in atomic p orbitals (for example, Bi $(6s^26p^3)$ and Se $(4s^24p^4)$) make the M_2X_3 compounds (M = Bi, Sb; X = Se, Te) function as topological insulators (TIs, recently discovered quantum materials that are insulating in the bulk, but conductive on the surface).

Based on the Bi_2Se_3 nanoribbons, which have larger surface-to-volume ratios than bulk materials and can therefore manifest surface effects, we show the first unambiguous transport evidence
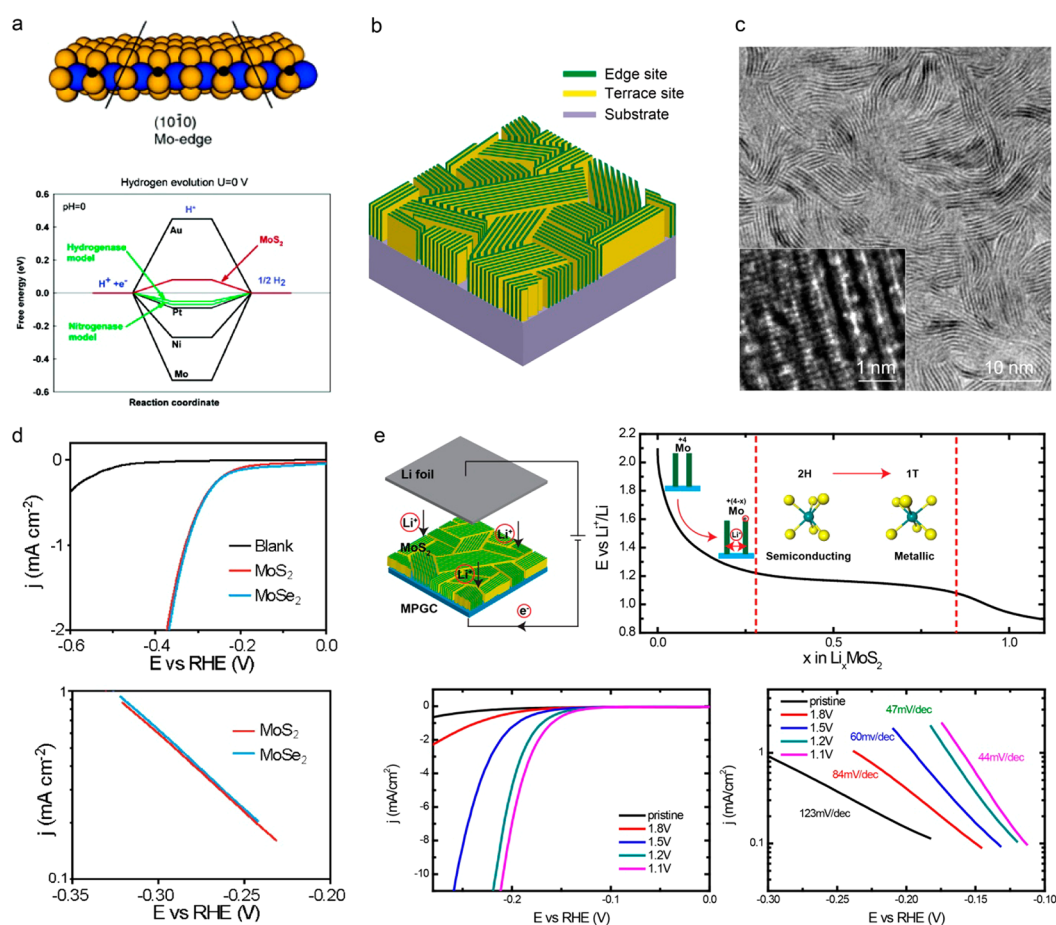
Figure 9. (a) Theoretical simulation of the free energy of H adsorption onto MoS_2 edge sites. Reproduced from ref 41. Copyright 2005 American Chemical Society. (b) Schematic of edge-terminated MoS_2 nanofilm. Reproduced from ref 42. Copyright 2013 American Chemical Society. (c) TEM image of edge-terminated MoS_2 nanofilm. Reproduced from ref 42. Copyright 2013 American Chemical Society. (d) HER performance of MoS_2 and $MoSe_2$ edge-terminated nanofilms. Reproduced from ref 43. Copyright 2013 American Chemical Society. (e) Li electrochemical tuning of MoS_2 nanofilms with the improved HER activities.[44−47] Panel e reproduced in part from ref 44. Copyright 2013 National Academy of Sciences.
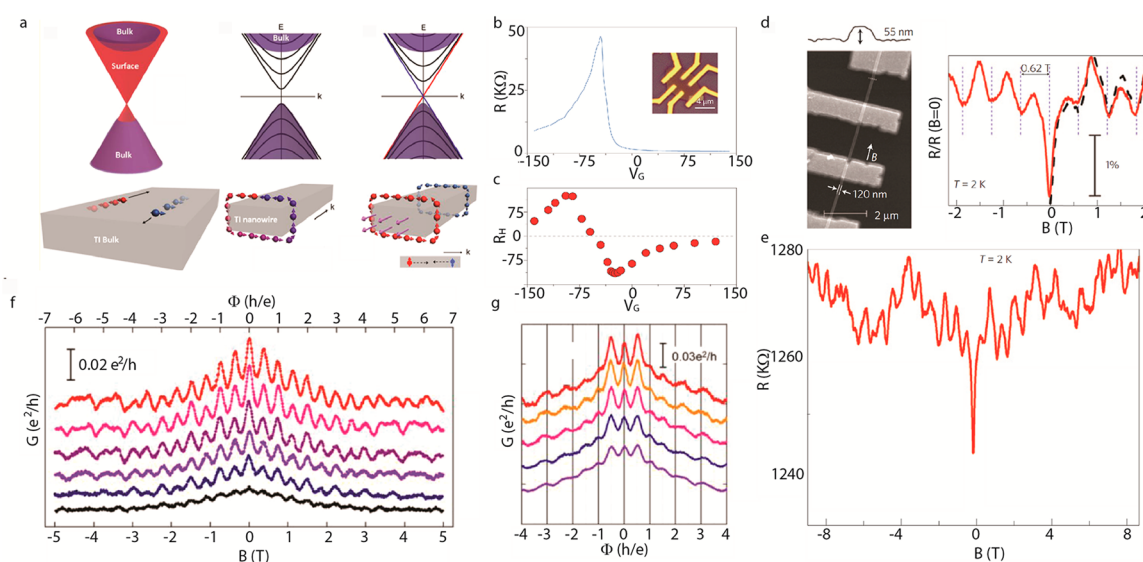

Figure 10. (a) Schematic band structure of 1D modes in Bi_2Se_3 nanowires. Reproduced from ref 50. Copyright 2014 American Chemical Society. (b, c) Ambipolar operation and the Hall coefficient in a field effect transistor based on $(Bi_xSb_{1−x})_2Te_3$ nanoribbons. Reproduced from ref 26. Copyright 2011 Nature Publishing Group. (d, e) Magnetoresistance as a function of the applied magnetic field, clearly indicating the Aharonov−Bohm effect in Bi_2Se_3 nanoribbons. Reproduced from ref 19. Copyright 2009 Nature Publishing Group. (f) Temperature-dependent quantum interferences of $h/(2e)$ period oscillations of a Bi_2Se_3 nanowire device. Reproduced from ref 50. Copyright 2014 American Chemical Society. (g) A representative quantum interference of a disordered Bi_2Se_3 nanowire device in parallel field at different temperatures. Reproduced from ref 50. Copyright 2014 American Chemical Society.

of topological surface states through periodic quantum interference effects (Figure 10). Pronounced Aharonov−Bohm oscillations in the magnetoresistance clearly demonstrate the coherent propagation of two-dimensional electrons around the perimeter of the nanoribbon surface, as expected from the topological nature of the surface states. The dominance of the primary h/e oscillation, where h is Planck's constant and e is the electron charge, and its temperature dependence demonstrate the robustness of these states. In the nanoribbon with sub-10 nm thickness, we can shift the Fermi levels of the top and bottom surfaces near the Dirac point by electrostatic gating, achieving extremely low two-dimensional carrier concentration of 2×10^{11} cm^{-2}. Therefore, we observed a topologically protected 1D mode of surface electrons in topological insulator nanowires existing at only two values of half magnetic quantum flux $(\pm h/(2e))$ due to a spin Berry's phase (π).[50] The helical 1D mode is robust against disorder but fragile against a perpendicular magnetic field (breaking-time-reversal symmetry), which demonstrates a device with robust and easily accessible 1D helical electronic states from 3D topological insulators.

Also the ternary sesquichalcogenides $(Bi_xSb_{1-x})_2Te_3$ and $Bi_2(Se_xTe_{1-x})_3$ are demonstrated to be a tunable topological insulator system in which we are able to engineer the bulk properties by changing the composition ratio.[24,26,50−52] With optimized ratio, we can reduce the bulk carrier density by over 2 orders of magnitude, while maintaining the topological insulator properties. As a result, we observe a clear ambipolar gating effect in $(Bi_xSb_{1-x})_2Te_3$ nanoplate field-effect transistor devices, similar to that observed in graphene field-effect transistors. The observation of the much more pronounced effect reported here benefits from the successful synthesis of ultrathin and low-density nanoplates, made possible by compositional engineering of the bulk carrier density in $(Bi_xSb_{1-x})_2Te_3$ compounds. An angle-dependent magnetoconductance study showed that an appropriate magnetic field range is critical to capture a true, two-dimensional weak antilocalization (WAL) effect, suggesting its origin may be the topological surface states.[24] Also, low-temperature transport measurements of the Fe-doped Bi_2Se_3 nanoribbon devices show a clear Kondo effect at temperatures below 30 K, confirming the presence of magnetic impurities in the Bi_2Se_3 nanoribbons.[23]

4.3. Optical Properties

New plasmonic materials with tunable properties are in great demand for nanophotonics and metamaterials applications, while the electron filling and orbital occupation control in 2D nanomaterials via intercalation affords opportunities for changing photonic properties. M_2X_3 chalcogenides were demonstrated as tunable metamaterials that feature both dielectric photonic and plasmonic modes across a wide spectral range from the infrared to the ultraviolet (Figure 11).[40] Monochromated electron energy-loss spectroscopy in a scanning transmission electron microscope was used to first establish the presence of the dielectric photonic and plasmonic modes in M_2X_3 nanoplates and to observe marked changes in these modes after chemical intercalation. We show that these modal properties can also be tuned effectively by geometric control and nanoplate composition.[40]

Interestingly, we discovered a counterintuitive result in the absorption properties of Cu-intercalated chalcogenide nanomaterials.[53] By intercalating Cu atoms, both absorption and reflection in layered Bi_2Se_3 and Bi_2Te_3 nanoplates are significantly reduced, resulting in extraordinary light transmission through thin nanoplates. The results highlight the interesting
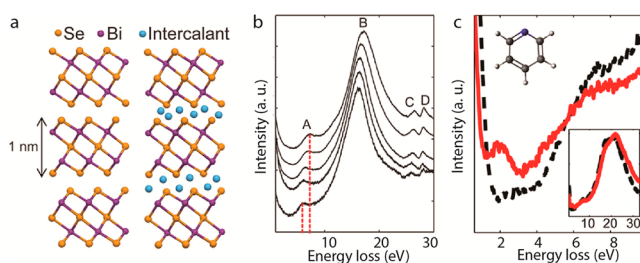

Figure 11. (a) Schematic diagram for the compositional control of $Bi_2(Se_xTe_{1-x})_3$ nanoribbons for plasmon tuning. (b) EELS spectra taken from $Bi_2(Se_xTe_{1-x})_3$ nanoribbons with different values of x. (c) EELS signal before (dotted black) and after (solid red) pyridine intercalation. Inset shows a pyridine molecule. Reproduced from ref 40. Copyright 2013 American Chemical Society.
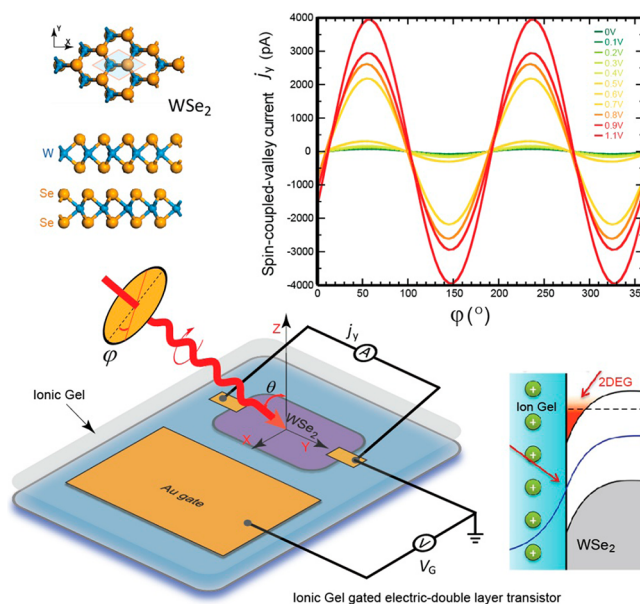

Figure 12. Generation and electric control of the spin-coupled valley photocurrent in ionic gel gated WSe_2 EDL transistors, based on the circular photogalvanic effect. Reproduced from ref 54. Copyright 2014 Nature Publishing Group.

photonic properties in chalcogenide nanomaterials, which can result from (1) tuning a large amount of carriers introduced by intercalation to effectively modulate absorption spectra beyond the original band gap and (2) the ultrasmall thickness of 2D nanomaterials, which is a significant factor for optical properties even for much longer wavelength range.

4.4. Valleytronics

Optical generation of spin and valley polarization by circularly polarized light in MX_2 chalcogenides (M = Mo, W; X = S, Se) with strong spin−orbit coupling is one of the most exciting topics since the valley degree of freedom in layered dichalcogenides can provide the opportunity to extend functionalities of novel spintronics and valleytronics devices.[12,54] If the nonequilibrium charge carrier imbalance between two degenerate and inequivalent valleys to realize valley/spin polarization can be obtained, we can realize the generation of a valley/spin current by the valley polarization in MX_2. Within an electric-double-layer transistor based on WSe_2, associated with the breaking of inversion symmetry (lower panel of Figure 12), we can generate a spin-coupled valley photocurrent whose direction and magnitude depend on the degree of circular polarization of the incident

radiation and can be further greatly modulated with an external electric field (Figure 12).[54]

The measurements induced by circularly polarized light on WSe_2 were used to detect a nonuniform distribution of photoexcited carriers and the generated spin current in WSe_2. When light is obliquely incident with a nonzero value, the obtained photocurrent exhibits a strong dependence on light circular polarization and oscillates with the rotation angle φ of the quarter wave plate (upper panel of Figure 12). Importantly, the photocurrent dramatically increases with external voltage from tens of picoamperes to thousands of picoamperes, unambiguously indicating an electric modulation of the spin current.[54] Such room temperature generation and electric control of valley/spin photocurrent provides a new property of electrons in MX_2 chalcogenides, thereby enabling new degrees of control for quantum-confined spintronics devices. More interesting, based on the large tunability of the EDLT and the achievement of ambipolar transport of chalcogenides, we also can realize the ambipolarity of the valley/spin photocurrent and related electric field modulation.[54]

5. CONCLUSION

This Account analyzes the rational design and chemical, electrochemical, and electrical modulations of the physical and chemical properties of layered nanomaterials via electron filling and orbital occupation control. Since the electron occupation of the orbitals in 2D layered materials controls the magnitude and anisotropy of the interatomic electron transfer and hence exerts a key influence on the chemical bonding modes of the 2D layered materials, we believe the modulation of orbital occupation and electron filling in 2D layered materials can provide us with a powerful way to achieve massive variations of their physical and chemical properties from catalysis and energy storage to superconductivity to spin−orbit coupling tuning and electronic, spintronic, and valleytronic applications.

■ AUTHOR INFORMATION

Corresponding Author

*E-mail: yicui@stanford.edu (Y.C.).

Notes

The authors declare no competing financial interest.

Biographies

Hongtao Yuan is a Research Associate at Geballe Laboratory for Advanced Materials in Stanford University and at Stanford Institute for Materials and Energy Sciences in SLAC National Accelerator Laboratory. He obtained his Ph.D. (2007) degree from Institute of Physics, Chinese Academic of Sciences. He was a postdoctoral researcher (2007−2010) at Institute of Materials Research (IMR), Tohoku University, and a research associate (2010−2011) and an assistant professor (2011−2012) at Quantum Phase Electronics Center (QPEC) in the University of Tokyo before joining Stanford University.

Haotian Wang is a graduate student in the Department of Applied Physics at Stanford University and currently a Stanford Interdisciplinary Graduate Fellow (SIGF). He obtained his B.S. (2011) in Physics at the University of Science and Technology of China. He is now supervised by Prof. Yi Cui and focused on applications of low-dimensional materials in catalysis, energy storage, and electronics and optoelectronics.

Yi Cui is a David Filo and Jerry Yang Faculty Scholar in the Department of Materials Science and Engineering and holds a courtesy appointment in the Department of Chemistry at Stanford University. He also holds a joint appointment in Photon Science Faculty, SLAC National Accelerator Laboratory. He obtained his B.S. in Chemistry from University of Science and Technology of China in 1998 and his Ph.D. in Chemistry in 2002 at Harvard University. He was awarded the prestigious Miller Postdoctoral Fellowship to work at the University of California, Berkeley. In 2005, he became an Assistant Professor at Stanford University and was awarded tenure at 2010.

■ REFERENCES

(1) Wilson, J. A.; Yoffe, A. D. Transition metal dichalcogenides discussion and interpretation of observed optical, electrical and structural properties. *Adv. Phys.* **1969**, *18*, 193−335.

(2) Chhowalla, M.; Shin, H. S.; Eda, G.; Li, L. J.; Loh, K. P.; Zhang, H. The chemistry of two-dimensional layered transition metal dichalcogenide nanosheets. *Nat. Chem.* **2013**, *5*, 263−275.

(3) Wang, Q. H.; Kalantar-Zadeh, K.; Kis, A.; Coleman, J. N.; Strano, M. S. Electronics and optoelectronics of two-dimensional transition metal dichalcogenides. *Nat. Nanotechnol.* **2012**, *7*, 699−712.

(4) Butler, S. Z.; Hollen, S. M.; Cao, L. Y.; Cui, Y.; Gupta, J. A.; Gutierrez, H. R.; Heinz, T. F.; Hong, S. S.; Huang, J.; Ismach, A. F.; Johnston-Halperin, E.; Kuno, M.; Plashnitsa, V. V.; Robinson, R. D.; Ruoff, R. S.; Salahuddin, S.; Shan, J.; Shi, L.; Spencer, M. G.; Terrones, M.; Windl, W.; Goldberger, J. E. Progress, challenges, and opportunities in two-dimensional materials beyond graphene. *ACS Nano* **2013**, *7*, 2898−2926.

(5) Tokura, Y.; Nagaosa, N. Orbital physics in transition-metal oxides. *Science* **2000**, *288*, 462−468.

(6) Hwang, H. Y.; Iwasa, Y.; Kawasaki, M.; Keimer, B.; Nagaosa, N.; Tokura, Y. Emergent phenomena at oxide interfaces. *Nat. Mater.* **2012**, *11*, 103−113.

(7) Xu, X. D.; Yao, W.; Xiao, D.; Heinz, T. F. Spin and pseudospins in layered transition metal dichalcogenides. *Nat. Phys.* **2014**, *10*, 343−350.

(8) Jaramillo, T. F.; Jorgensen, K. P.; Bonde, J.; Nielsen, J. H.; Horch, S.; Chorkendorff, I. Identification of active edge sites for electrochemical H_2 evolution from MoS_2 nanocatalysts. *Science* **2007**, *317*, 100−102.

(9) Radisavljevic, B.; Radenovic, A.; Brivio, J.; Giacometti, V.; Kis, A. Single-layer MoS_2 transistors. *Nat. Nanotechnol.* **2011**, *6*, 147−150.

(10) Georgiou, T.; Jalil, R.; Belle, B. D.; Britnell, L.; Gorbachev, R. V.; Morozov, S. V.; Kim, Y. J.; Gholinia, A.; haigh, S. J.; Makarovsky, O.; Eaves, L.; Ponomarenko, L. A.; Geim, A. K.; Novoselov, K. S.; Mishchenko, A. Vertical field-effect transistor based on graphene-WS_2 heterostructures for flexible and transparent electronics. *Nat. Nanotechnol.* **2013**, *8*, 100−103.

(11) Kim, S.; Konar, A.; Hwang, W. S.; Lee, J. H.; Lee, J.; Yang, J.; Hung, C.; Kim, H.; Yoo, J. B.; Choi, j. Y.; Jin, Y. W.; Lee, S. Y.; Jena, D.; Choi, D.; Kim, K. High-mobility and low-power thin-film transistors based on multilayer MoS_2 crystals. *Nat. Commun.* **2012**, *3*, 1011.

(12) Yuan, H. T.; Bahramy, M. S.; Morimoto, K.; Wu, S.; Nomura, K.; Yang, B.-J.; Shimotani, H.; Suzuki, R.; Toh, M.; Kloc, C.; Xu, X. D.; Arita, R.; Nagaosa, N.; Iwasa, Y. Zeeman-type spin splitting controlled by an electric field. *Nat. Phys.* **2013**, *9*, 563−569.

(13) Geim, A. K.; Grigorieva, I. V. Van der Waals heterostructures. *Nature* **2013**, *499*, 419−425.

(14) Novoselov, K. S.; Geim, A. K.; Morozov, S. V.; Jiang, D.; Katsnelson, M. I.; Grigorieva, I. V.; Dubonos, S. V.; Firsov, A. A. Two-dimensional gas of massless Dirac fermions in graphene. *Nature* **2005**, *438*, 197−200.

(15) Chen, Y. L.; Analytis, J. G.; Chu, J. H.; Liu, Z. K.; Mo, S. K.; Qi, X. L.; Zhang, H. J.; Lu, D. H.; Dai, X.; Fang, Z.; Zhang, S. C.; Fisher, I. R.; Hussain, Z.; Shen, Z. X. Experimental realization of a three-dimensional topological insulator, Bi_2Te_3. *Science* **2009**, *325*, 178−181.

(16) Yazyev, O. V.; Kioupakis, E.; Moore, J. E.; Louie, S. G. Quasiparticle effects in the bulk and surface-state bands of Bi_2Se_3 and Bi_2Te_3 topological insulators. *Phys. Rev. B* **2012**, *85*, No. 161101.

(17) Wagner, R. S.; Ellis, W. C. Vapor-liquid-solid mechanism of single crystal growth. *Appl. Phys. Lett.* **1964**, *4*, 89−90.

(18) Cui, Y.; Lauhon, L. J.; Gudiksen, M. S.; Wang, J. F.; Lieber, C. M. Diameter-controlled synthesis of single-crystal silicon nanowires. *Appl. Phys. Lett.* **2001**, *78*, 2214−2216.

(19) Peng, H. L.; Lai, K. J.; Kong, D. S.; Meister, S.; Chen, Y. L.; Qi, X. L.; Zhang, S. C.; Shen, Z. X.; Cui, Y. Aharonov-Bohm interference in topological insulator nanoribbons. *Nat. Mater.* **2010**, *9*, 225−229.

(20) Peng, H. L.; Xie, C.; Schoen, D. T.; Cui, Y. Large anisotropy of electrical properties in layer-structured In$_2$Se$_3$ nanowires. *Nano Lett.* **2008**, *8*, 1511−1516.

(21) Meister, S.; Peng, H. L.; McIlwrath, K.; Jarausch, K.; Zhang, X. F.; Cui, Y. Synthesis and characterization of phase-change nanowires. *Nano Lett.* **2006**, *6*, 1514−1517.

(22) Kong, D. S.; Randel, J. C.; Peng, H. L.; Cha, J. J.; Meister, S.; Lai, K. J.; Chen, Y. L.; Shen, Z. X.; Manoharan, H.; Cui, Y. Topological insulator nanowires and nanoribbons. *Nano Lett.* **2010**, *10*, 329−333.

(23) Cha, J. J.; Claassen, M.; Kong, D. S.; Hong, S. S.; Koski, K. J.; Qi, X. L.; Cui, Y. Effects of magnetic doping on weak antilocalization in narrow Bi$_2$Se$_3$ nanoribbons. *Nano Lett.* **2012**, *12*, 4355−4359.

(24) Cha, J. J.; Kong, D. S.; Hong, S. S.; Analytis, J. G.; Lai, K. J.; Cui, Y. Weak antilocalization in Bi$_2$(Se$_x$Te$_{1-x}$)$_3$ nanoribbons and nanoplates. *Nano Lett.* **2012**, *12*, 1107−1111.

(25) Kong, D. S.; Dang, W. H.; Cha, J. J.; Li, H.; Meister, S.; Peng, H. L.; Liu, Z. F.; Cui, Y. Few-layer nanoplates of Bi$_2$Se$_3$ and Bi$_2$Te$_3$ with highly tunable chemical potential. *Nano Lett.* **2010**, *10*, 2245−2250.

(26) Kong, D. S.; Chen, Y. L.; Cha, J. J.; Zhang, Q. F.; Analytis, J. G.; Lai, K. J.; Liu, Z. K.; Hong, S. S.; Koski, K. J.; Mo, S. K.; Hussain, Z.; Fisher, I. R.; Shen, Z. X.; Cui, Y. Ambipolar field effect in the ternary topological insulator (Bi$_x$Sb$_{1-x}$)$_2$Te$_3$ by composition tuning. *Nat. Nanotechnol.* **2011**, *6*, 705−709.

(27) Schoen, D. T.; Peng, H.; Cui, Y. Anisotropy of chemical transformation from In$_2$Se$_3$ to CuInSe$_2$ nanowires through solid state reaction. *J. Am. Chem. Soc.* **2009**, *131*, 7973−7975.

(28) Schoen, D. T.; Peng, H.; Cui, Y. CuInSe$_2$ nanowires from facile chemical transformation of In$_2$Se$_3$ and their integration in single-nanowire devices. *ACS Nano* **2013**, *7*, 3205−3211.

(29) Frindt, R. F. Single crystals of MoS$_2$ several molecular layers thick. *J. Appl. Phys.* **1966**, *37*, 1928.

(30) Frindt, R. F. Superconductivity in ultrathin NbSe$_2$ layers. *Phys. Rev. Lett.* **1972**, *28*, 299−301.

(31) Hong, S. S.; Kundhikanjana, W.; Cha, J. J.; Lai, K. J.; Kong, D. S.; Meister, S.; Kelly, M. A.; Shen, Z. X.; Cui, Y. Ultrathin topological insulator Bi$_2$Se$_3$ nanoribbons exfoliated by atomic force microscopy. *Nano Lett.* **2010**, *10*, 3118−3122.

(32) Yuan, H. T.; Shimotani, H.; Tsukazaki, A.; Ohtomo, A.; Kawasaki, M.; Iwasa, Y. High-density carrier accumulation in ZnO field-effect transistors gated by electric double layers of ionic liquids. *Adv. Funct. Mater.* **2009**, *19*, 1046−1053.

(33) Yuan, H. T.; Toh, M.; Morimoto, K.; Tan, W.; Wei, F.; Shimotani, H.; Kloc, Ch.; Iwasa, Y. Liquid-gated electric-double-layer transistor on layered metal dichalcogenide, SnS$_2$. *Appl. Phys. Lett.* **2011**, *98*, No. 012102.

(34) Ye, J. T.; Inoue, S.; Kobayashi, K.; Kasahara, Y.; Yuan, H. T.; Shimotani, H.; Iwasa, Y. Liquid-gated interface superconductivity on an atomically flat film. *Nat. Mater.* **2010**, *9*, 125−128.

(35) Hor, Y. S.; Williams, A. J.; Checkelsky, J. G.; Roushan, P.; Seo, J.; Xu, Q.; Zandbergen, H. W.; Yazdani, A.; Ong, N. P.; Cava, R. J. Superconductivity in Cu$_x$Bi$_2$Se$_3$ and its implications for pairing in the undoped topological insulator. *Phys. Rev. Lett.* **2010**, *104*, No. 057001.

(36) Peng, H. L.; Zhang, X. F.; Twesten, R. D.; Cui, Y. Vacancy ordering and lithium insertion in III$_2$VI$_3$ Nanowires. *Nano Res.* **2009**, *2*, 327−335.

(37) Koski, K. J.; Cha, J. J.; Reed, B. W.; Wessells, C. D.; Kong, D. S.; Cui, Y. High-density chemical intercalation of zero-valent copper into Bi$_2$Se$_3$ Nanoribbons. *J. Am. Chem. Soc.* **2012**, *134*, 7584−7587.

(38) Koski, K. J.; Wessells, C. D.; Reed, B. W.; Cha, J. J.; Kong, D.; Cui, Y. Chemical intercalation of zerovalent metals into 2D layered Bi$_2$Se$_3$ Nanoribbons. *J. Am. Chem. Soc.* **2012**, *134*, 13773−13779.

(39) Motter, J. P.; Koski, K. J.; Cui, Y. General strategy for zero-valent intercalation into two-dimensional layered nanomaterials. *Chem. Mater.* **2014**, *26*, 2313−2317.

(40) Cha, J. J.; Koski, K. J.; Huang, K. C. Y.; Wan, K. X.; Luo, W. D.; Kong, D. S.; Yu, Z. F.; Fan, S. H.; Brongersma, M. L.; Cui, Y. Two-dimensional chalcogenide nanoplates as tunable metamaterials via chemical intercalation. *Nano Lett.* **2013**, *13*, 5913−5918.

(41) Hinnemann, B.; Moses, P. G.; Bonde, J.; Jørgensen, K. P.; Nielsen, J. H.; Horch, S.; Chorkendorff, I.; Norskov, J. K. Biomimetic hydrogen evolution: MoS$_2$ nanoparticles as catalyst for hydrogen evolution. *J. Am. Chem. Soc.* **2005**, *127*, 5308−5309.

(42) Kong, D.; Wang, H.; Cha, J. J.; Pasta, M.; Koski, K. J.; Yao, J.; Cui, Y. Synthesis of MoS$_2$ and MoSe$_2$ films with vertically aligned layers. *Nano Lett.* **2013**, *13*, 1341−1347.

(43) Wang, H.; Kong, D.; Johanes, P.; Cha, J. J.; Zheng, G.; Yan, K.; Liu, N.; Cui, Y. MoSe$_2$ and WSe$_2$ nanofilms with vertically aligned molecular layers on curved and rough surfaces. *Nano Lett.* **2013**, *13*, 3426−3433.

(44) Wang, H.; Lu, Z.; Xu, S.; Kong, D.; Cha, J. J.; Zheng, G.; Hsu, P. C.; Yan, K.; Bradshaw, D.; Prinz, F. B.; Cui, Y. Electrochemical tuning of vertically aligned MoS$_2$ nanofilms and its application in improving hydrogen evolution reaction. *Proc. Natl. Acad. Sci. U. S. A.* **2013**, *110*, 19701−19706.

(45) Wang, H.; Lu, Z.; Kong, D.; Sun, J.; Hymel, T. M.; Cui, Y. Electrochemical tuning of MoS$_2$ nanoparticles on three-dimensional substrate for efficient hydrogen evolution. *ACS Nano* **2014**, *8*, 4940−4947.

(46) Lukowski, M. A.; Daniel, A. S.; Meng, F.; Forticaux, A.; Li, L.; Jin, S. Enhanced hydrogen evolution catalysis from chemically exfoliated metallic MoS$_2$ nanosheets. *J. Am. Chem. Soc.* **2013**, *135*, 10274−10277.

(47) Voiry, D.; Yamaguchi, H.; Li, J.; Silva, R.; Alves, D. C. B.; Fujita, T.; Chen, M. W.; Asefa, T.; Shenoy, V. B.; Eda, G.; Chhowalla, M. Enhanced catalytic activity in strained chemically exfoliated WS$_2$ nanosheets for hydrogen evolution. *Nat. Mater.* **2013**, *12*, 850−855.

(48) Lu, Z.; Wang, H.; Kong, D.; Yan, K.; Hsu, P.-C.; Zheng, G.; Yao, H. B.; Liang, Z.; Sun, X. M.; Cui, Y. Electrochemical tuning of layered lithium transition metal oxides for improvement of oxygen evolution reaction. *Nat. Commun.* **2014**, *5*, No. 4345.

(49) Maiyalagan, T.; Jarvis, K. A.; Therese, S.; Ferreira, P. J.; Manthiram, A. Spinel-type lithium cobalt oxide as a bifunctional electrocatalyst for the oxygen evolution and oxygen reduction reactions. *Nat. Commun.* **2014**, *5*, No. 3949.

(50) Hong, S. S.; Zhang, Y.; Cha, J. J.; Qi, X. L.; Cui, Y. One-dimensional helical transport in topological insulator nanowire interferometers. *Nano Lett.* **2014**, *14*, 2815−2821.

(51) Kong, D. S.; Koski, K. J.; Cha, J. J.; Hong, S. S.; Cui, Y. Ambipolar field effect in Sb-doped Bi$_2$Se$_3$ nanoplates by solvothermal synthesis. *Nano Lett.* **2013**, *13*, 632−636.

(52) Hong, S. S.; Cha, J. J.; Kong, D. S.; Cui, Y. Ultra-low carrier concentration and surface-dominant transport in antimony-doped Bi$_2$Se$_3$ topological insulator nanoribbons. *Nat. Commun.* **2012**, *3*, No. 757.

(53) Yao, J.; Koski, K. J.; Luo, W. D.; Cha, J. J.; Hu, L. B.; Kong, D. S.; Narasimhan, K. S.; Huo, K. F.; Cui, Y. Optical transmission enhacement through chemically tuned two-dimensional bismuth chalcogenide nanoplates. *Nat. Commun.* **2014**, *5*, No. 5670.

(54) Yuan, H. T.; Wang, X. Q.; Lian, B.; Zhang, H. J.; Fang, X. F.; Shen, B.; Xu, G.; Xu, Y.; Zhang, S. C.; Hwang, H. Y.; Cui, Y. Generation and electric control of spin-valley-coupled circular photogalvanic current in WSe$_2$. *Nat. Nanotechnol.* **2014**, *9*, 851−857.